Sea surface temperature cooling mode in the Pacific cold tongue

Wenjun Zhang,[1,2] Jianping Li,[2] and Xia Zhao[2,3]

Received 2 July 2010; revised 28 September 2010; accepted 4 October 2010; published 17 December 2010.

[1] Long-term variability in sea surface temperature (SST) in the equatorial Pacific and its relationship with global warming were investigated using three SST data sets (Hadley Center Global Sea Ice and Sea Surface Temperature, extended reconstruction sea surface temperature, and Kaplan), atmospheric fields from National Centers for Environmental Prediction/National Center for Atmospheric Research reanalysis, and subsurface sea temperature from the Simple Ocean Data Assimilation data set. A cooling mode in the equatorial Pacific cold tongue is evident in all three SST data sets for two periods: 1870–2007 and 1948–2007. This cooling, which is indicated by the second empirical orthogonal function mode, is characterized by cooling in the Pacific cold tongue and warming elsewhere in the tropical Pacific. Its principal component time series is highly correlated with global mean surface temperature combining air temperature and SST. In association with the SST cooling mode, atmospheric fields and subsurface sea temperature are coupled in the tropical Pacific during recent decades. Moreover, for the coupled models in the 20th century run (20C3M), obtained from the Intergovernmental Panel on Climate Change Fourth Assessment Report database, those with realistic features of El Niño-Southern Oscillation (ENSO) events can well show the cooling mode. However, the cooling mode is not shown in these coupled models in a preindustrial scenario with no forcing attributed to global warming. Results from observations and models suggest that the cooling mode is very likely caused by global warming. This conclusion is supported by a hypothesis that considers dynamic effects in the equatorial Pacific Ocean in response to global warming.

Citation: Zhang, W., J. Li, and X. Zhao (2010), Sea surface temperature cooling mode in the Pacific cold tongue, *J. Geophys. Res.*, *115*, C12042, doi:10.1029/2010JC006501.

1. Introduction

[2] The El Niño-Southern Oscillation (ENSO), a phenomenon driven by coupled air-sea processes, is the most prominent interannual variability on Earth [*Philander*, 1990; *McPhaden et al.*, 2006] and exhibits a degree of predictability on the seasonal-to-interannual time scales [*Latif et al.*, 1998; *Chen et al.*, 2004]. Although ENSO originates in the tropical Pacific, ENSO-related climate anomalies are observed at a global scale [e.g., *Trenberth et al.*, 1998; *Wallace et al.*, 1998; *Wu et al.*, 2009]. Within the three most recent decades, two intense El Niño episodes have occurred (1982 and 1997), as well as more central Pacific El Niño events that have action centers located primarily in the central Pacific [*Ashok et al.*, 2007; *Kug et al.*, 2009; *Kao and Yu*, 2009; *Yu and Kim*, 2010].

[3] *Fedorov and Philander* [2000] indicated that global warming is sure to affect ENSO by altering the background climate. Thus, long-term variability of sea surface temperature (SST) in the tropical Pacific requires additional study to better understand ENSO changes associated with global warming. Another reason for such study is that long-term variability in SST in the tropical Pacific Ocean may have a large impact on global climate. The tropical Pacific Ocean is a central driver of climate because it provides a substantial portion of global atmospheric sensible and latent heat [*Cane*, 1998].

[4] Nevertheless, the relationship between climate change in the tropical Pacific and global warming is controversial: is warming greater in the east relative to the west, or vice versa? On the one hand, a warming trend with an El Niño-like pattern in the tropical Pacific has been identified in recent decades from observations [*Graham*, 1995; *Wang*, 1995; *Trenberth and Hoar*, 1996; *Zhang et al.*, 1997; *Knutson and Manabe*, 1998] and simulations [*Knutson and Manabe*, 1995; *Tett*, 1995; *Meehl and Washington*, 1996; *Roeckner et al.*, 1996; *Timmermann et al.*, 1999; *Cai and Whetton*, 2000; *Jin et al.*, 2001]. On the other hand, an increase in the SST zonal gradient across the equatorial Pacific has been shown in long-term SST analyses [*Cane et al.*, 1997; *Karnauskas et al.*, 2009], simulations [*Noda*

[1]Key Laboratory of Meteorological Disaster of Ministry of Education and College of Atmospheric Sciences, Nanjing University of Information Science and Technology, Nanjing, China.
[2]State Key Laboratory of Numerical Modeling for Atmospheric Sciences and Geophysical Fluid Dynamics, Institute of Atmospheric Physics, Chinese Academy of Sciences, Beijing, China.
[3]Laboratory of Ocean Circulation and Waves, Institute of Oceanology, Chinese Academy of Sciences, Qingdao, China.

0148-0227/10/2010JC006501

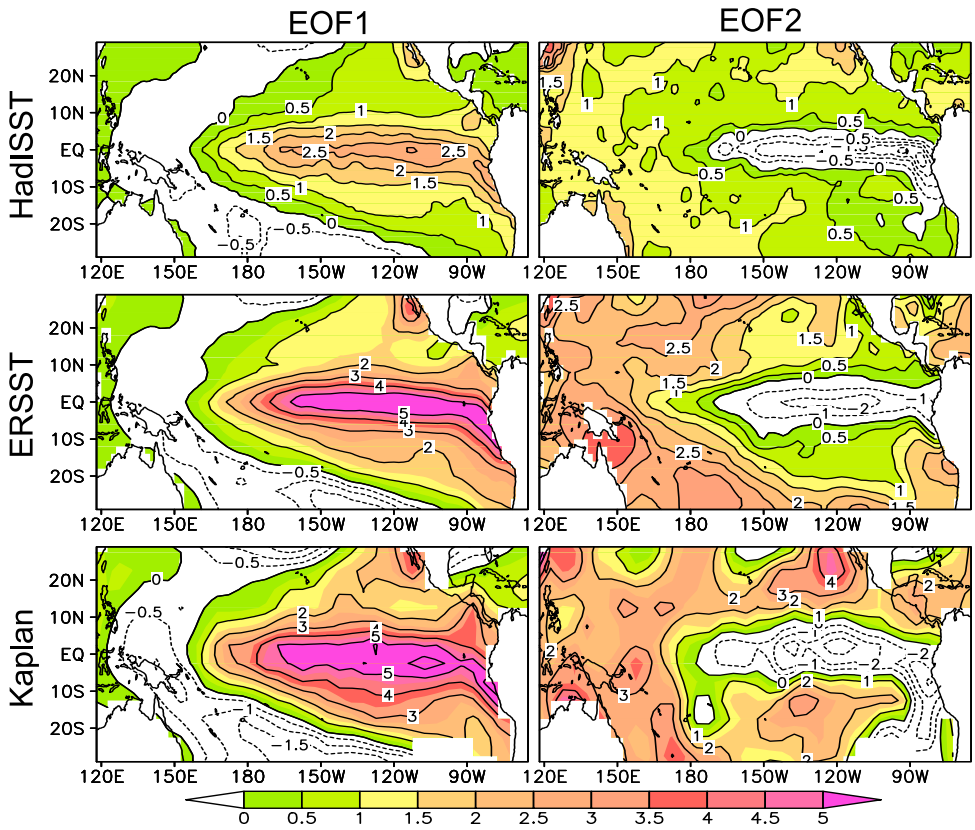

Figure 1. The SST EOF1 (left) and EOF2 (right) for the HadISST (top), ERSST (middle), and Kaplan (bottom) data sets.

et al., 1999], and theoretical studies [*Clement et al.*, 1996; *Cane et al.*, 1997; *Seager and Murtugudde*, 1997].

[5] Recently, a multimodel ensemble did not predict a large-amplitude shift toward mean El Niño-like or La Niña-like conditions [*Collins et al.*, 2005]. These controversies arise partly from conflicting hypotheses about mean climate change [e.g., *Knutson and Manabe*, 1995; *Pierrehumbert*, 1995; *Sun and Liu*, 1996; *Cane et al.*, 1997; *Clement and Seager*, 1999]. These hypotheses deal with the relative roles of different feedback involved in the climate response to greenhouse warming in the tropical Pacific.

[6] A cloud-albedo feedback may cause SST warming to be greater in the eastern tropical Pacific than in the western tropical Pacific as a result of less incoming solar radiation caused by a stronger cloud shielding effect in the west than in the east [e.g., *Meehl and Washington*, 1996]. A dynamic feedback of the equatorial Pacific Ocean indicates that stronger warming will occur in the western equatorial Pacific because larger amounts of subsurface cool water brought up to the surface by strong equatorial upwelling would inhibit the warming rate in the cold tongue region [e.g., *Cane et al.*, 1997]. Recently, *Karnauskas et al.* [2009] suggested that both mechanisms are at work, but with relative strengths that vary seasonally. Overall, the mechanisms controlling the mean state of the tropical Pacific are not fully understood. However, its mean state is important as an indicator for predicting future atmospheric circulation. Additional studies are necessary for understanding long-term variations in the tropical Pacific.

[7] In this study, long-term SST variability in the cold tongue strip is examined by analyzing a cooling mode in the equatorial Pacific cold tongue strip obtained from the second empirical orthogonal function (EOF) mode in SST (Figures 1 and 2). This cooling mode shows cooling trends in SST in the cold tongue region and the increasingly strong zonal gradient in SST across the equatorial Pacific, which is opposite to trends in global warming. However, it is uncertain whether changes in mean SST in the tropical Pacific could be resolved based on SST data. For example, long-term trends are suspect in the Lamont-Doherty Earth Observatory optimal smoothing SST analysis (Kaplan SST) [*Hurrell and Trenberth*, 1999].

[8] Therefore, comparisons among different data sets from different periods are used in this study to identify the cooling mode in the cold tongue region. Coupled phenomena in atmospheric circulation and subsurface sea temperature, as well as simulations in coupled general circulation models (CGCMs), are also investigated. Finally, a possible linkage is discussed between the cooling mode and global warming.

2. Data Sets

[9] The monthly SST data sets (1870–2006) used in this study include the Hadley Center Global Sea Ice and Sea

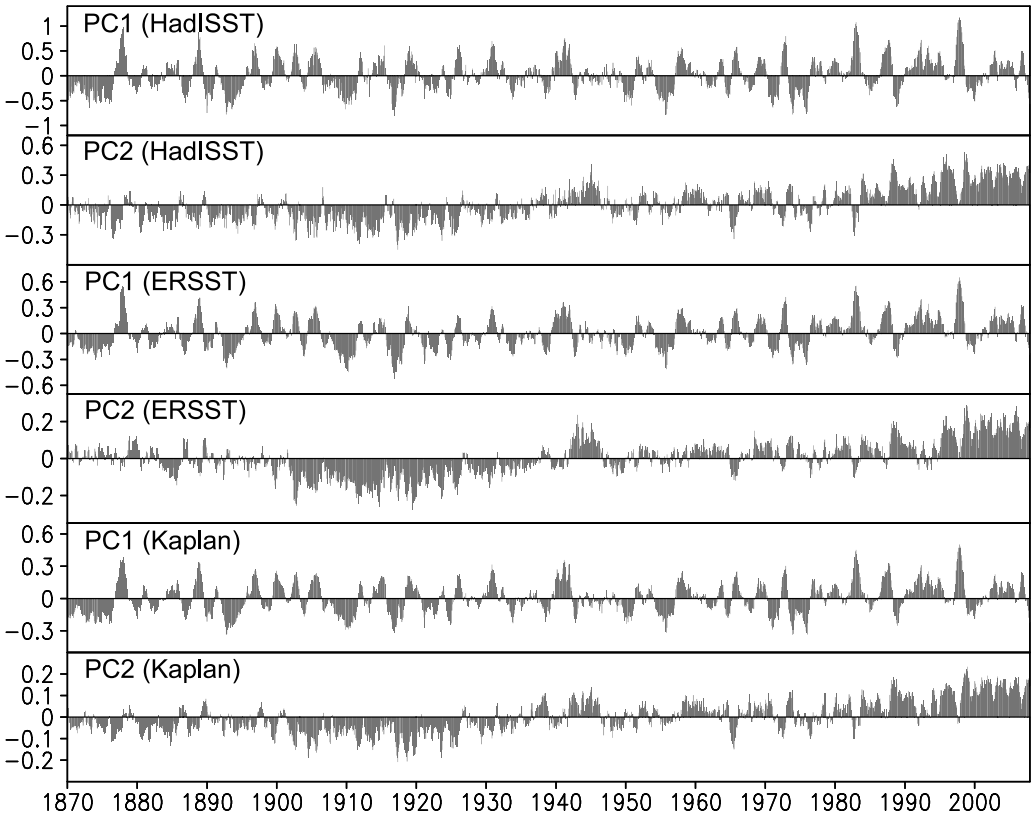

Figure 2. PCs corresponding to EOF1 and EOF2 modes in Figure 1.

Surface Temperature (HadISST) Analyses data sets [*Rayner et al.*, 2003], the extended reconstruction sea surface temperature (ERSST) data set [*Smith and Reynolds*, 2004] from the NOAA Climate Diagnostics Center, and the Kaplan SST data set [*Kaplan et al.*, 1998]. Monthly subsurface sea temperature data are from the Simple Ocean Data Assimilation (SODA) data set (1958–2004) [*Carton et al.*, 2000]. The horizontal resolutions are, respectively, 1° × 1°, 2° × 2°, 5° × 5°, and 0.5° × 0.5° for the HadISST, ERSST, Kaplan, and SODA data sets. We also used the third Met Office Hadley Centre and Climatic Research Unit Global Land and Sea Surface Temperature Data Set (HadCRUT3) [*Brohan et al.*, 2006].

[10] The atmospheric general circulation data sets are taken from the National Centers for Environmental Prediction/National Center for Atmospheric Research (NCEP/NCAR) reanalysis products [*Kalnay et al.*, 1996]. The data used in this study include horizontal and vertical velocity and sea level pressure (SLP). These variables are gridded at 2.5° latitude × 2.5° longitude resolution and are available from 1948 to 2007. All the data sets used in this study describe anomalies: the mean seasonal cycle from 1961 to 1990 has been removed unless otherwise noted.

[11] In this study, we also examine whether the cooling mode occurs in CGCMs included in the Intergovernmental Panel on Climate Change (IPCC) Fourth Assessment Report (AR4) database. Model references can be obtained from the IPCC website (http://www-pcmdi.llnl.gov/ipcc/model_documentation/ipcc_model_documentation.php). We choose the 100 year (1900–1999) results for the 20th century run (20C3M) and the last 50 year results for the preindustrial (picntrl) scenario.

3. Leading SST Modes and Their Long-Term Changes in the Tropical Pacific

[12] To identify spatial and temporal features in SST variability in the tropical Pacific, EOF analysis was applied to monthly SST anomalies (SSTA) in the three SST data sets used in this study. Figures 1 and 2 show the first two leading modes and their corresponding principal components (PCs). For the HadISST data set, the first two modes account for 40.1% and 10.0% of the total variance, respectively (Table 1). They are well separated from each other according to the criterion of *North et al.* [1982]. The pattern of the first mode captures the well-known El Niño pattern in the tropical Pacific [*Rasmusson and Carpenter*, 1982]. By combining EOF1 with its related PC, we observe some typical El Niño years, such as 1982 and 1997, as well as more El Niño events in the most recent three decades. This mode mainly presents interannual variability in the tropical Pacific.

Table 1. Fraction of Variance Explained by the Main EOF Modes

	1870–2007		1948–2007	
	Mode 1	Mode 2	Mode 1	Mode 2
HadISST	40.1%	10.0%	40.0%	10.0%
ERSST	37.5%	11.0%	41.8%	9.5%
Kaplan	35.9%	10.0%	35.0%	9.1%

Table 2. Correlation Coefficients for PCs Between the HadISST, ERSST, and Kaplan Data Sets[a]

		PC1			PC2		
		HadISST	ERSST	Kaplan	HadISST	ERSST	Kaplan
1870–2007	HadISST	1.00	0.94	0.97	1.00	0.84	0.93
	ERSST	-	1.00	0.96	-	1.00	0.86
	Kaplan	-	-	1.00	-	-	1.00
1948–2007	HadISST	1.00	0.98	0.99	1.00	0.54	0.63
	ERSST	-	1.00	0.98	-	1.00	0.93
	Kaplan	-	-	1.00	-	-	1.00

[a]All correlation coefficients are statistically significant at the 99% level.

[13] In the second mode and its corresponding PC, warming appears almost everywhere in the tropical Pacific, with notable exceptions in the cold tongue, which is a result similar to the cooling trend in the cold tongue reported in a previous study [*Cane et al.*, 1997]. This mode clearly displays the long-term variability in SST in the tropical Pacific. These phenomena are also presented in the ERSST and Kaplan data sets (Figures 1 and 2). The patterns of the first two SST modes for the ERSST and Kaplan products are almost the same as those of the HadISST data, and their corresponding PCs are highly correlated with those of the HadISST data (Table 2). Although differences exist among SST products because of contrasting analysis techniques [*Hurrell and Trenberth*, 1999], the ENSO variability and the SST cooling mode are apparent in all three SST analyses. Note that the robustness of the EOF patterns was examined by confining the meridional domain to 20°S–20°N in the three SST data. Even for the meridional domain expanded to 40°S–40°N, the EOF2 patterns and the associated variances explained do not change significantly. Also the cooling modes can be displayed in the domain confined in the eastern tropical Pacific.

[14] The PC2 time series in the three SST data sets consistently indicate a weak decline from 1870 to about 1910, a rise to 1945, a slight decline to about 1970, and a rise to the present (Figure 2), which is consistent with the long-term variability in global mean land surface temperature and SST. The correlation between the PC2 time series and the HadCRUT3 global mean surface temperature is shown in Table 3. There is a strong positive correlation between the PC2 time series of the three data sets (HadISST, ERSST, and Kaplan) and the global warming signal represented by the HadCRUT3 surface temperature, especially for the 7 year low-pass filtered time series (Table 3).

[15] This correlation indicates that the EOF2 modes may be associated with global warming. However, the response of SST to global warming is not homogeneous in the equatorial Pacific. SST in the west is warming, while SST in the east is cooling, in the equatorial Pacific in the EOF2 mode (Figure 1). Why are the SST changes associated with global warming not consistent throughout the equatorial Pacific? We will discuss a possible physical mechanism in section 6.

[16] For the post-1948 period, the cooling mode can also be obtained from EOF analysis in the three SST data sets (Figures 3 and 4 and Tables 1 and 2), as also mentioned by *Lau and Weng* [1999]. The spatial correlation coefficients are high (above 0.7) between the EOF2 patterns of 1948–2007 and those of 1870–2007 for all three SST data sets. Also, there are strong positive correlations (above 0.88) between the PC2 time series of 1948–2007 and those of 1870–2007 during the overlapping period in the three SST data sets. However, some differences appear near the equatorial South America in the EOF2 mode: the HadISST data set shows cooling, whereas the other two data sets show warming. As a whole, the three different products consistently show a cooling mode in the main cold tongue region for the post-1948 period, and high correlation coefficients are found between their PC2 time series and the global mean surface temperature (Table 3), similar to that for the post-1870 period.

4. Coupled Phenomena Associated With the SST Cooling Mode

[17] Because of strong ocean-atmosphere interactions in the tropical Pacific, atmospheric circulation and subsurface temperature may exhibit coupled characteristics associated with the SST cooling mode. To further confirm the SST cooling mode in the cold tongue strip, regression analysis in Figure 5 was performed to study the association between the cooling mode and five fields, including subsurface sea temperature, and four atmospheric circulation fields (the surface zonal and meridional winds, SLP, and pressure velocity). The analyses presented here use atmospheric data from 1948 to 2007, but subsurface temperature data from 1958 to 2004, constrained by the SODA data record.

[18] Figure 5 shows the regression patterns of the five fields on the normalized PC2 time series of the HadISST SSTA in the 1948–2007 period. In association with the cooling cold tongue as shown in Figure 3, anomalous divergence of surface winds occurs at low levels, with southwesterly and northwesterly wind anomalies, respectively, to the north and south of the SST cooling region (Figure 5a). Over the western equatorial Pacific, easterly wind anomalies prevail to the west of the date line. Simul-

Table 3. Correlation Coefficients Between the PC2 Time Series and HadCRU3 Global Mean Surface Temperature for Original and 7 Year Low-Pass Filtered Time Series[a]

	Original Time Series		7 Year Low-Pass Filtered Time Series	
	1870–2007	1948–2007	1870–2007	1948–2007
HadISST	0.72	0.59	0.96	0.91
ERSST	0.65	0.67	0.88	0.91
Kaplan	0.72	0.70	0.94	0.95

[a]All correlation coefficients are statistically significant at the 99% level.

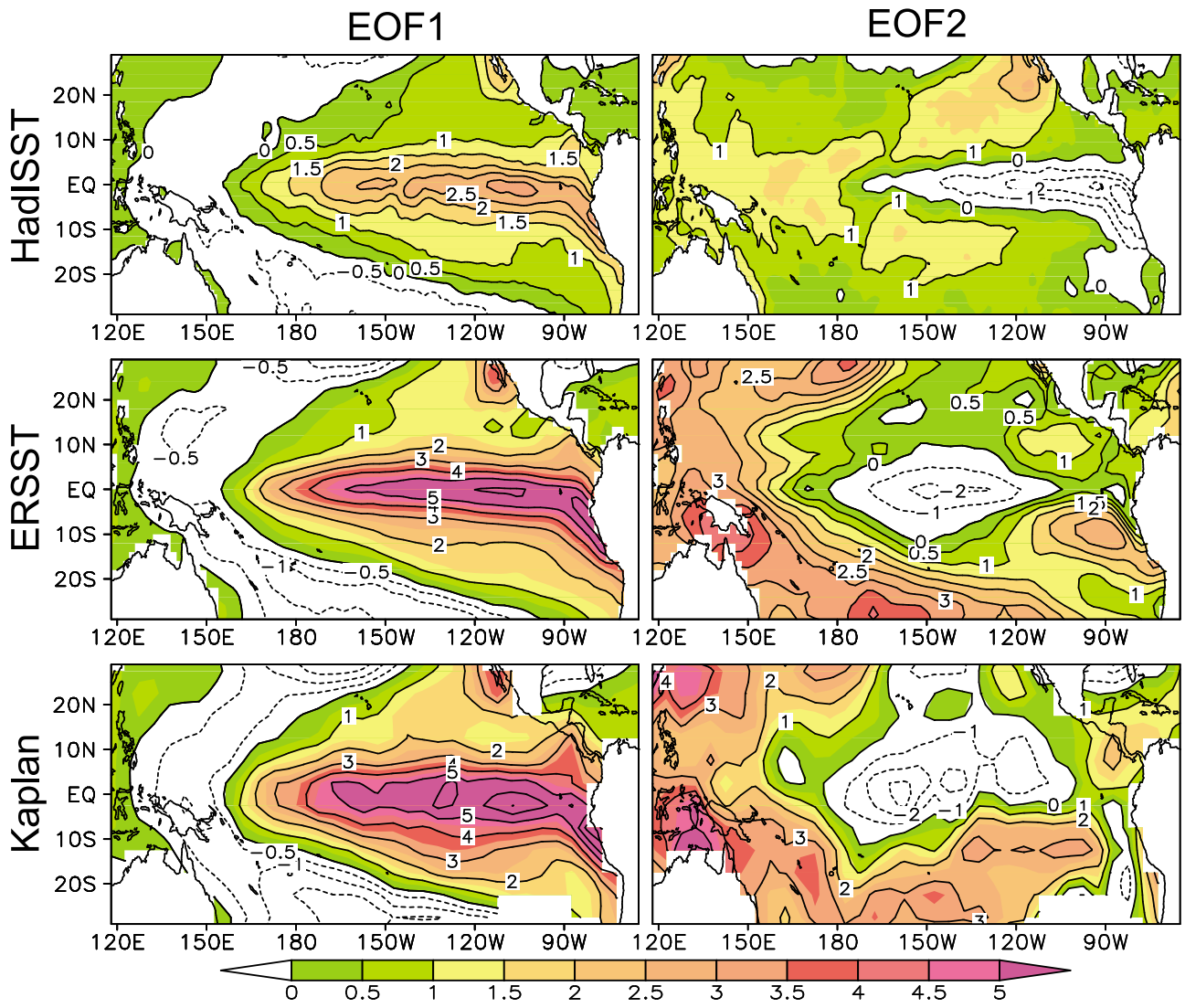

Figure 3. As in Figure 1, except for 1948–2007.

taneously, anomalous atmospheric sinking appears over the central and eastern equatorial Pacific related to the SST cooling mode (Figure 5b). The sinking center is located over the central equatorial Pacific, and it can reach 200 hPa. Apparently, the divergent atmospheric circulation is coupled to the cooling SST in the cold tongue region.

[19] Corresponding to the cooling mode in the Pacific cold tongue, SLP exhibits an increase over almost the entire equatorial Pacific (Figure 5c), which is similar to the results of *Thompson et al.* [2000] and *Gillett et al.* [2003], and is possibly caused by external forcing, such as from greenhouse gases, stratospheric ozone depletion, volcanic aerosols, and solar forcing [*Gillett et al.*, 2005]. Although SLP rises over almost the entire equatorial Pacific, significantly positive anomalies are mainly located over the eastern equatorial Pacific, because of divergent circulation associated with the cooling SST there. Meanwhile, the subsurface temperature above 120 m is cooling in the east and warming in the west of the equatorial Pacific (Figure 5d), which is well coupled with the SST cooling mode displayed in Figure 3. As shown in Figure 5, the different fields in the equatorial Pacific are coupled well with the SST cooling mode. We also investigate the regression maps of the atmospheric and subsurface temperature fields on the PC2 time series of the ERSST and Kaplan data. Their regression patterns (data not shown) are similar to those in Figure 5.

5. Simulated Results in Coupled Models

[20] The ocean components of previous CGCMs were run at resolutions too coarse to resolve the equatorial oceans [*Knutson and Manabe*, 1995]. Recent models tend to be more realistic in representing the frequency with which ENSO occurs, and they are better at locating enhanced temperature variability in the eastern Pacific Ocean, as shown by the results of the Coupled Model Intercomparison Project [*AchutaRao and Sperber*, 2002, 2006]. These improvements may be partly attributed to improved resolution. It would be interesting to investigate whether the cooling mode in SST can be reproduced by recent models. Here, we inspect this feature based on the coupled models in

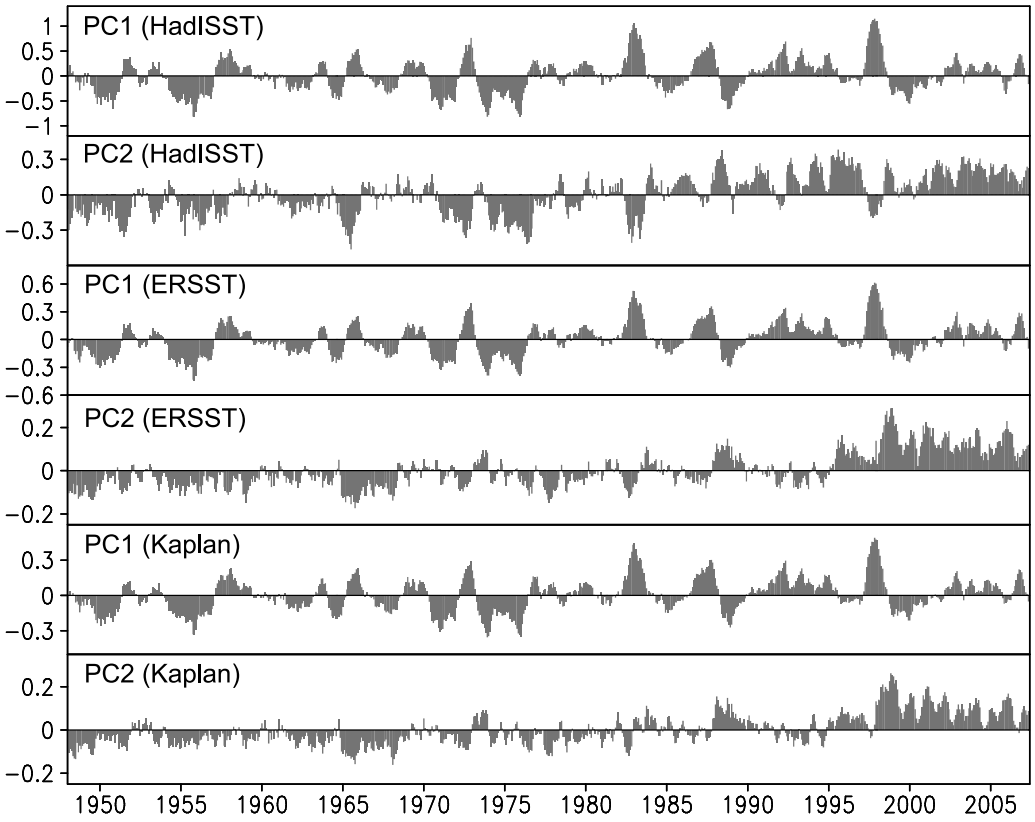

Figure 4. As in Figure 2, except for 1948–2007.

the 20C3M scenario, and the HadISST and ERSST data sets are used for reference.

[21] EOF analysis is applied to monthly SSTA in which the SST seasonal cycle has been removed from the period of interest (Figures 6 and 7). EOF1 modes in the tropical Pacific, and the corresponding PCs, are shown in Figure 6. The ENSO variability in the two observed SST EOFs in the 1900–1999 period is very similar to the results displayed in Figure 1. However, ENSO variability cannot be captured by all of the coupled models (Figure 6), and the first six models (the two CGCM3.1, GISS-AOM, GISS-ER, and two MIROC3.2 models) show no significant interannual variability and are dominated by a rising trend in SST. Modeled ENSO amplitudes in these models are lower than or equal to about half the value of the observed variability (Figure 8). Especially for the GISS-AOM and GISS-ER models, there are almost no interannual signals. Since the interannual signal is too weak in these models, dynamic processes in the tropical Pacific cannot be realistically reproduced, and it is possible that their primary variability is masked by global warming. In the other models, ENSO variability is reasonably shown in their leading EOF modes. Nevertheless, Figure 6 shows that some models appear to have problems in simulating the interannual variability in the equatorial Pacific related to, for example, having too strong an interannual variability in the western equatorial Pacific (CSIRO-Mk3.0 and INM-CM3) or too regular an ENSO cycle (e.g., FGOALS-g1.0).

[22] For the HadISST and ERSST data sets, EOF2 modes and corresponding PCs show the SST cooling mode in the cold tongue strip (Figure 7), which is also displayed in Figure 1. The observed spatial pattern of the EOF2 modes is realistically reproduced by most models. Figure 8 shows that the PC2 time series exhibit a positive trend in all models, except for the GISS-ER model. However, the PC2 time series are dominated by high-frequency variability in about half of the models, which is not consistent with those of the observations. In comparison, the PC2 time series associated with the observed EOF2 mode are well simulated by about one-third of the models. These models that have realistic ENSO features in EOF1 can better reproduce the observed long-term variability associated with the EOF2 modes compared to the other models, except for the UKMO-HadCM3 model (Figure 8). Especially, six models (CCSM3, CNRM-CM3, GFDL-CM2.0, GISS-EH, IPSL-CM4, and MRI-CGCM2.3.2) simulate well the observed long-term variability in the equatorial Pacific. The trends are relatively weak in the ECHAM5/MPI and parallel climate model models. Overall, the SST cooling mode in the equatorial cold tongue region can also be identified in the coupled models that show reasonable ENSO variability.

6. Possible Relationships Between the SST Cooling Mode and Global Warming

[23] As mentioned in section 3, the strong correlation between the PC2 time series and global mean surface temperature suggests that the cooling mode is linked with global warming. In discussing long-term changes in SST in the tropical Pacific associated with global warming, *Cane et al.*

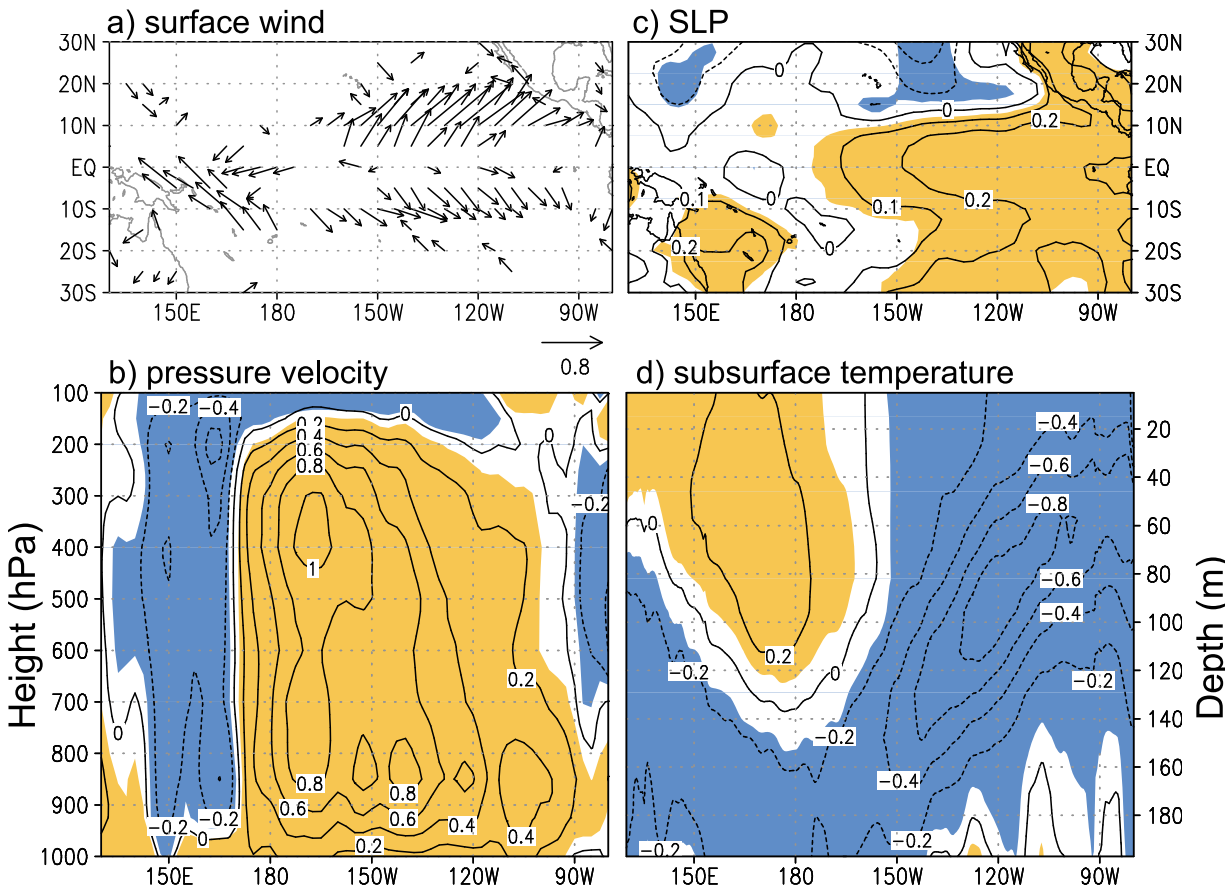

Figure 5. Anomalies of (a) surface wind (m/s), (b) pressure velocity (mean from 5°S to 5°N; 10^{-2} pa/s), (c) SLP (hPa), and (d) subsurface temperature (mean from 5°S to 5°N; °C) regressed upon the normalized PC2 time series of the HadISST SSTA in the 1948–2007 period (shown in Figure 4). The analyses use atmospheric data from 1948 to 2007 but subsurface temperature data from 1958 to 2004, constrained by the SODA data record. Shading indicates the correlation coefficients exceeding the 95% confidence level. Only values in Figure 5a that are statistically significant at the 95% confidence level are shown.

[1997] emphasized the effects of dynamic feedback and characterized this feedback process as follows:

> "In the eastern equatorial region, however, vigorous upwelling brings up cold water from below, counteracting the warming tendency. Thus, initially, the SST increases more in the west than in the east, enhancing the temperature gradient along the equator. The atmosphere responds with increasing trade winds, which in turn will increase the upwelling rate and the thermocline tilt, cooling the surface waters in the east and further enhancing the temperature contrast…."

[24] However, the long-term trends of 20th century SST exhibit an inconsistent behavior in the eastern equatorial Pacific between different reconstructed data sets. *Deser et al.* [2010] pointed out that the HadISST1 and Kaplan data sets disagree with the ERSST and uninterpolated data sets on the sing of the SST trend in the eastern equatorial Pacific, although these SST data sets exhibit broad similarity in their trend patterns and amplitudes in other regions. These uncertainties are possibly caused by sparse observations before the 1950s. Furthermore, we investigate the trends in SST since the 1950s, for which period the density of SST observations is adequate to allow analysis (Figure 9). In the 1950–2007 period, the ERSST data set also shows an inconsistent feature in the SST trends in the eastern equatorial Pacific compared to the HadISST1 and Kaplan data sets. The ERSST data set displays significant warming in the eastern equatorial Pacific, while the trends are weak and not significant for the HadISST1 and Kaplan data sets. Although uncertainties of SST trends appear in the eastern equatorial Pacific, the three data sets consistently show the increasingly strong east-west SST gradient across the equatorial Pacific. The SST gradient also increases in all the three data sets in the 1980–2007 period. Interestingly, warming occurs in the west while cooling occurs in the east in this period.

[25] Since greenhouse gas forcing has very likely caused most of the observed global warming during the latter half of the 20th century [*Hegerl et al.*, 2007], why does the equatorial Pacific SST exhibit inconsistent trends between the east and west under the external forcing? It seems, possibly, that the dynamic feedback can be used to explain the stronger warming in the western equatorial Pacific relative to the eastern equatorial Pacific. However, difficulties remain in separating the contributions of natural and anthropogenic forcings to global warming in the observations over the time scale of several decades. Considering the

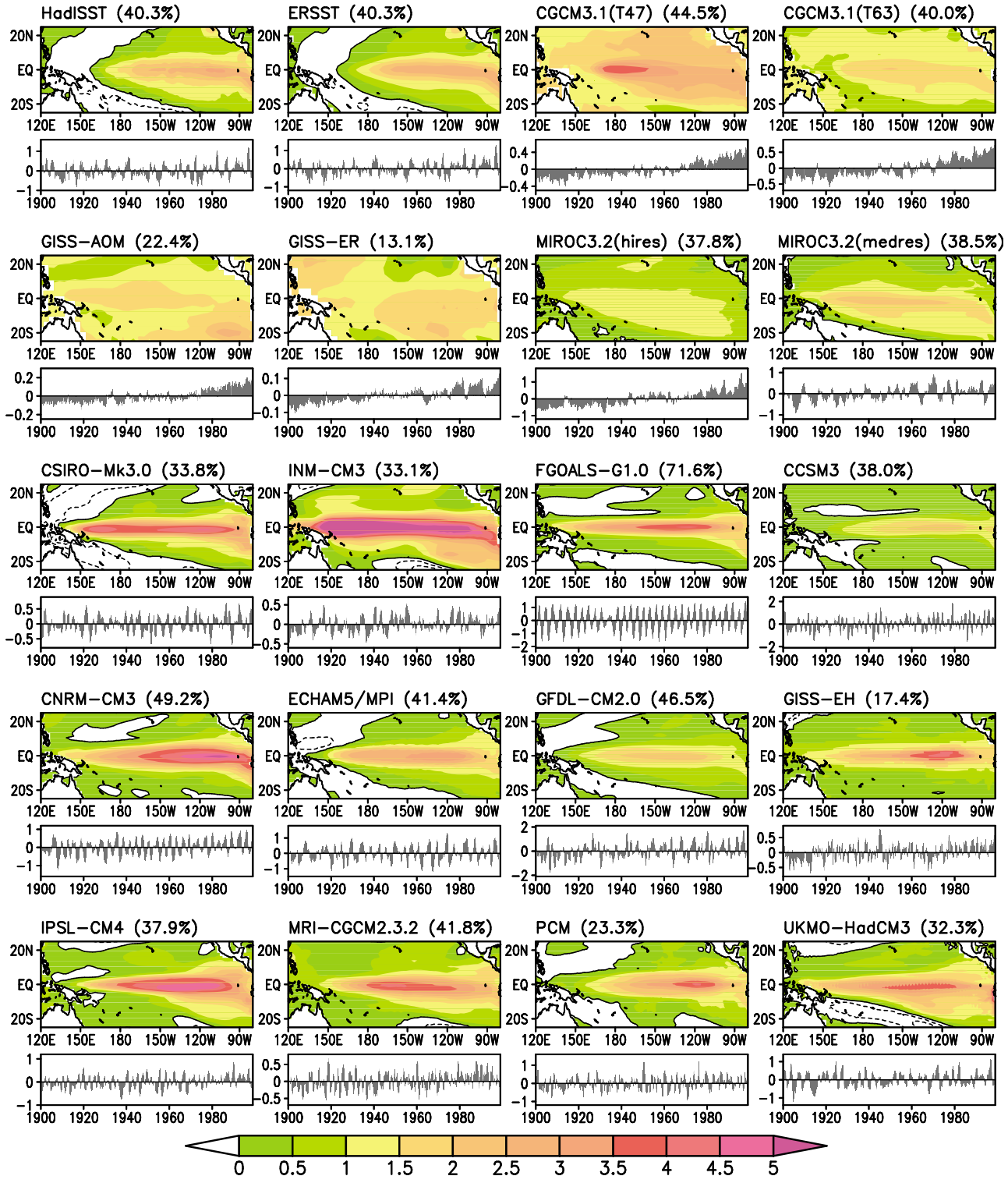

Figure 6. The leading EOF modes in SST in the tropical Pacific (30°S–30°N, 115°E–80°W) and their corresponding PC time series for the 20C3M simulations. The dashed line denotes negative values. The contour interval is 0.5°C. The models' names and variances are shown above each EOF mode.

ocean interior processes emphasized in the dynamic feedback, we further investigate the associating changes in the subsurface layer of the equatorial Pacific Ocean in the 20C3M scenario. In this section, we selected six models (CCSM3, CNRM-CM3, GFDL-CM2.0, GISS-EH, IPSL-CM4, and MRI-CGCM2.3.2) to discuss their changes in the subsurface layer, since they perform well in reproducing the ENSO and cooling modes in 20C3M. Figure 10 shows the trends of modeled subsurface temperature in the western and eastern equatorial Pacific. The trends of ocean temperature

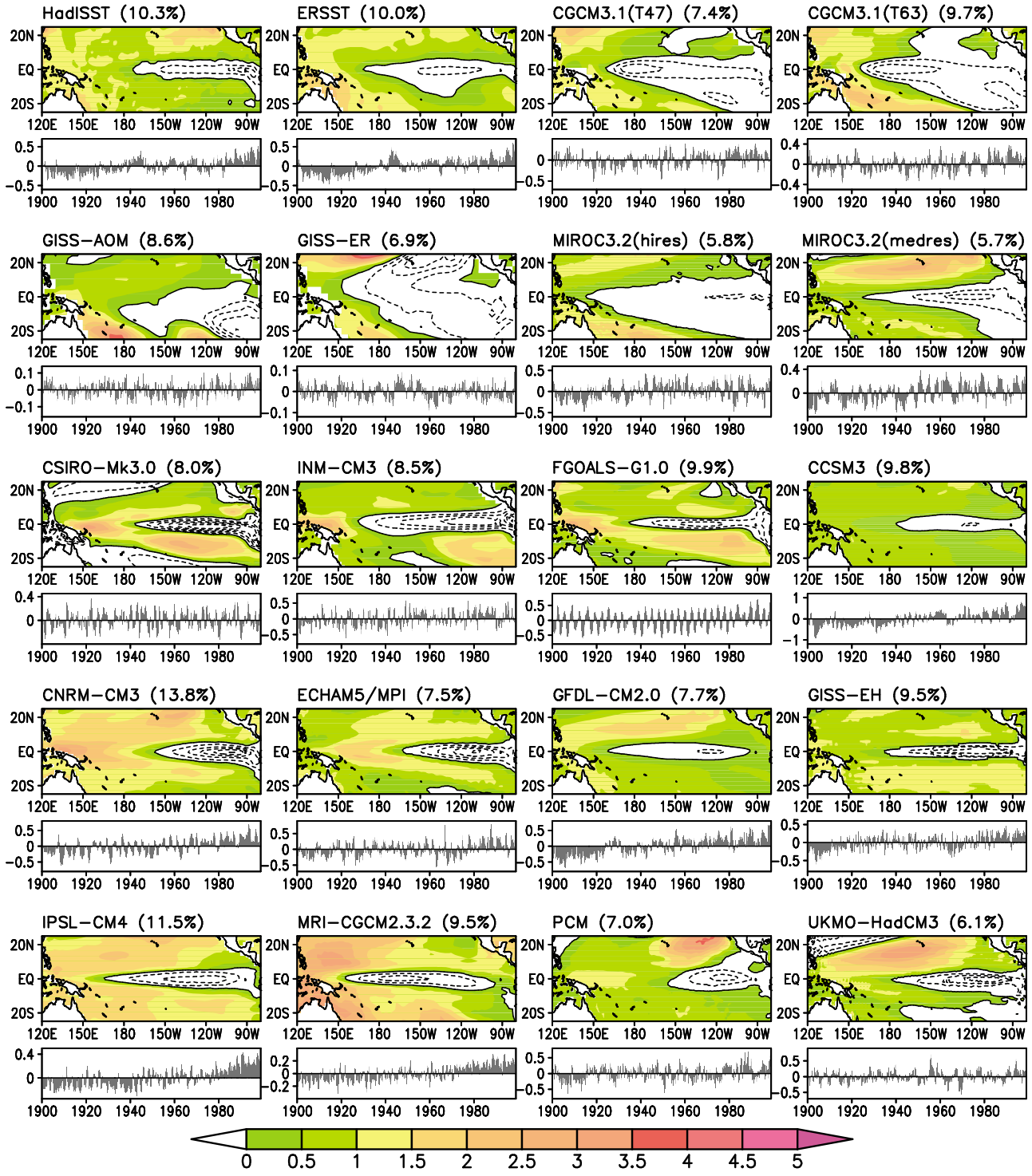

Figure 7. As in Figure 6, except for the second EOF modes and their corresponding PC time series.

are weaker at thermocline (generally being 150 and 60 m, respectively, in the western and eastern equatorial Pacific) than those at surface layer in all the six models. Therefore, the vertical gradients of the ocean temperature above the thermocline are strengthened in both the eastern and western equatorial Pacific during the 20th century. In the eastern equatorial Pacific, strong upwelling can bring up cold water from below, inhibiting the surface warming rate, while this ocean dynamic process does not occur in the western equatorial Pacific in the absence of vigorous upwelling. As shown in Figure 10, the trends of ocean temperature in the eastern equatorial Pacific are weaker than those in the western equatorial Pacific near the thermocline of the eastern equatorial Pacific in all six models, except for the GFDL-CM2.0 model. Similarly, four models (CNRM-CM3, GISS-EH, IPSL-CM4, and MRI-CGCM2.3.3) pres-

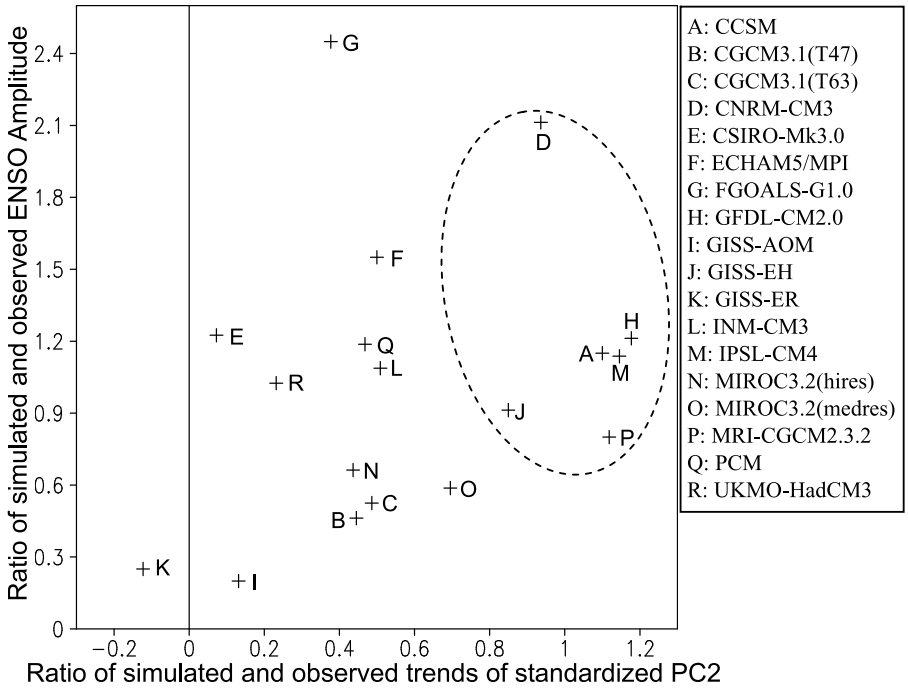

Figure 8. The ratio of ENSO amplitude as a function of the ratio of trends of the standardized PC2 time series between the 20C3M simulations and the observations. The models in the circle are those that realistically reproduce the ENSO variability and better simulate the observed trend associated with the EOF2 modes compared to the other models. The ENSO amplitude is defined as the standard deviation in SST in the central and eastern equatorial Pacific (5°S–5°N, 180°–90°W). The HadISST data set is used for reference.

ent that the trends of the surface ocean temperature are weaker in the east than those in the west of the equatorial Pacific. In the CCSM3 model, however, stronger warming appears in the east than in the west, and the inconsistency is possibly attributed to the simulated difficulties of the coupled system at the ocean-atmosphere interface [e.g, *Neelin et al.*, 1994].

[26] Since the temperature gradient near the thermocline of the eastern equatorial Pacific is stronger across the equatorial Pacific in models, their upwelling is expected to increase in the eastern equatorial Pacific according to the dynamic feedback proposed by *Cane et al.* [1997]. Figure 11 displays the trends of upwelling in the eastern equatorial Pacific in three models available. The upwelling in all three models increases along with global warming above the thermocline, with the strongest trend near the thermocline. Overall, the results of models suggest that the dynamic feedback very likely plays an important role in the equatorial Pacific along with global warming.

[27] The dynamic feedback is also possibly reflected by the SST cooling mode indicated by the EOF2 mode. That is, the SST cooling mode is possibly caused by dynamic feedback in response to global warming. To investigate further, we inspected the simulations of coupled models in the picntrl scenario, in which there is no forcing because of global warming. As shown in Figure 12, the six models can realistically show ENSO variability, which is similar to the case in Figure 6. However, their EOF2 modes do not show the cooling modes, because their PCs are dominated by interannual variability. A comparison of results between the 20C3M and picntrl scenarios reveals that the cooling mode coexists with global warming in the coupled models. Therefore, the cooling mode is most likely the result of global warming through the dynamic feedback process in the equatorial Pacific Ocean.

7. Conclusions

[28] Long-term variability in SST in the equatorial Pacific was investigated using three different SST data sets (HadISST, ERSST, and Kaplan), atmospheric fields (NCEP/NCAR reanalysis), and subsurface sea temperature (SODA) data. In addition to the first EOF mode (ENSO mode), the cooling mode in the Pacific cold tongue can be obtained from these SST data sets for two periods (1870–2007 and 1948–2007) as the second mode, indicating a cooling trend in the Pacific cold tongue and a warming trend elsewhere in the tropical Pacific. These findings are similar to the results of *Cane et al.* [1997] and *Lau and Weng* [1999]. Corresponding to the cooling mode, atmospheric fields and subsurface sea temperatures exhibit coupled characteristics in the past several decades. The divergent atmospheric circulation is coupled to the cooling SST, and subsurface temperatures are cooling in the east and warming in the west over the equatorial Pacific. Moreover, the coupled models from the IPCC AR4 20C3M run, which realistically simulate ENSO variability, also well display the cooling mode.

[29] The PCs associated with the cooling mode in the three SST data sets (HadISST, ERSST, and Kaplan) are highly correlated with the global average surface tempera-

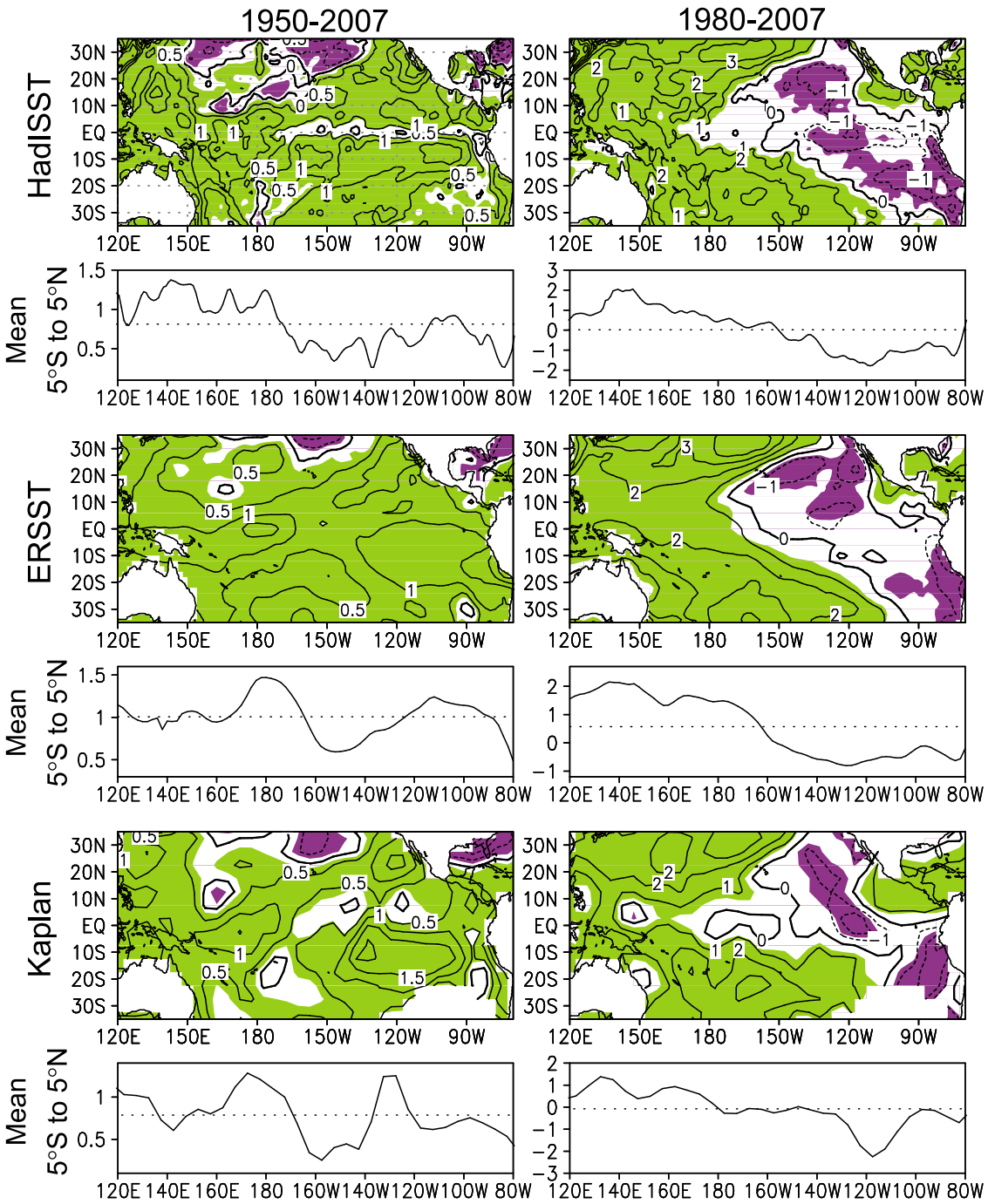

Figure 9. Spatial patterns and mean values (averaged from 5°S to 5°N) in trends (in °C per 100 years) in monthly mean SSTA for the periods 1950–2007 (left) and 1980–2007 (right) in the HadISST (top), ERSST (middle), and Kaplan (bottom) data sets. Regions over the 0.05 confidence level are shaded, and dashed lines denote negative values. The dotted lines are values averaged from 120°E to 80°W.

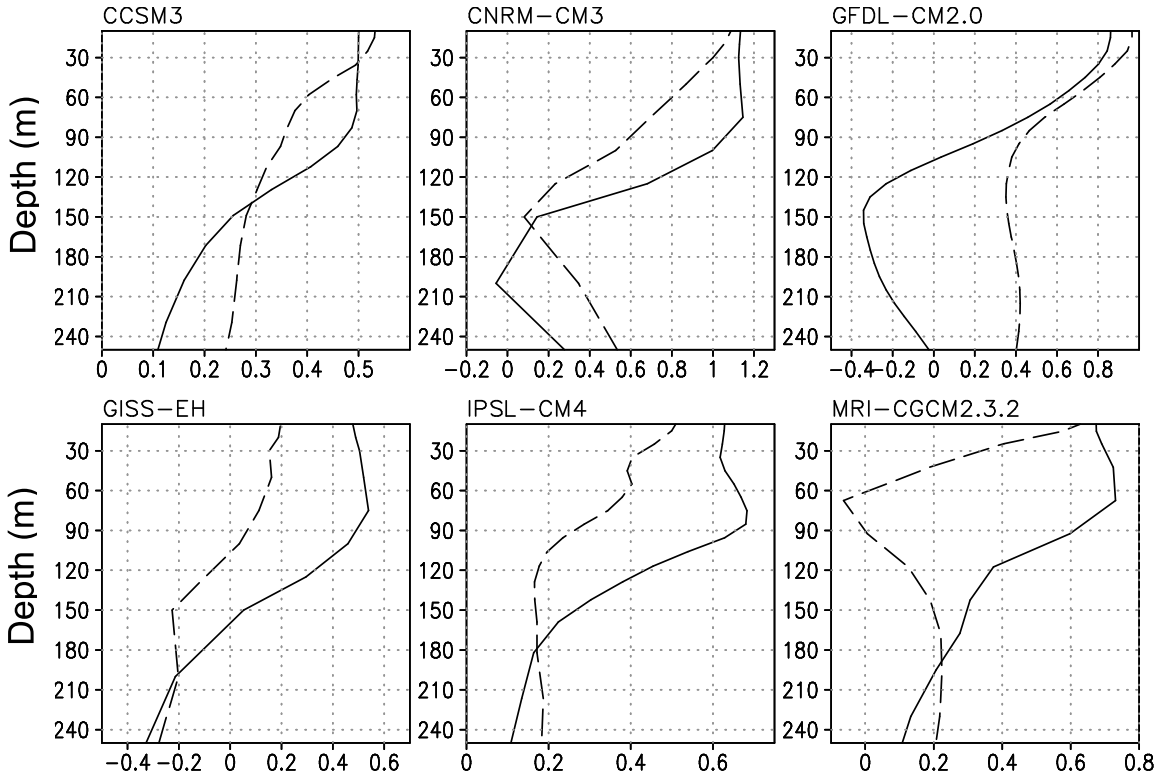

Figure 10. The trends (in °C per 100 years) of subsurface temperature over the western equatorial Pacific (2°S–2°N, 130°–180°E; solid lines) and the eastern equatorial Pacific (2°S–2°N, 90°–150°W; dashed lines).

ture. Furthermore, in the 20C3M run the cooling mode is well reproduced by six coupled models with well performance in simulating the two leading EOF modes, but it disappears in the picntrl run. These results, based on observations and models, indicate that the cooling mode in the cold tongue region may be associated with global warming, possibly reflecting the dynamic effect (i.e., increasing upwelling) in the eastern equatorial Pacific Ocean, as suggested by *Cane et al.* [1997]. This dynamic effect is also possibly indicated by an increasingly strong east-west SST gradient in the equatorial Pacific during the latter half of the 20th century. In the 20C3M run, the ocean temperature increases more in the west than in the east near the thermocline of the eastern equatorial Pacific in the six models selected, and their gradient of ocean temperature is enhanced along the equatorial Pacific in these models. Simultaneously, the increasingly strong upwelling appears above the thermocline layer in three models available. These results in the

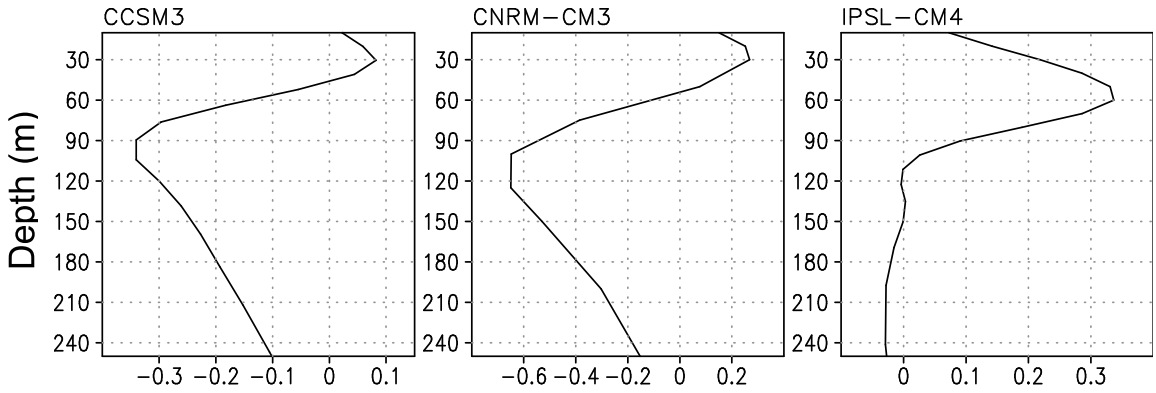

Figure 11. The trends (in 10^{-6} m/s per 100 years) of upwelling over the eastern equatorial Pacific (2°S–2°N, 90°W–180°).

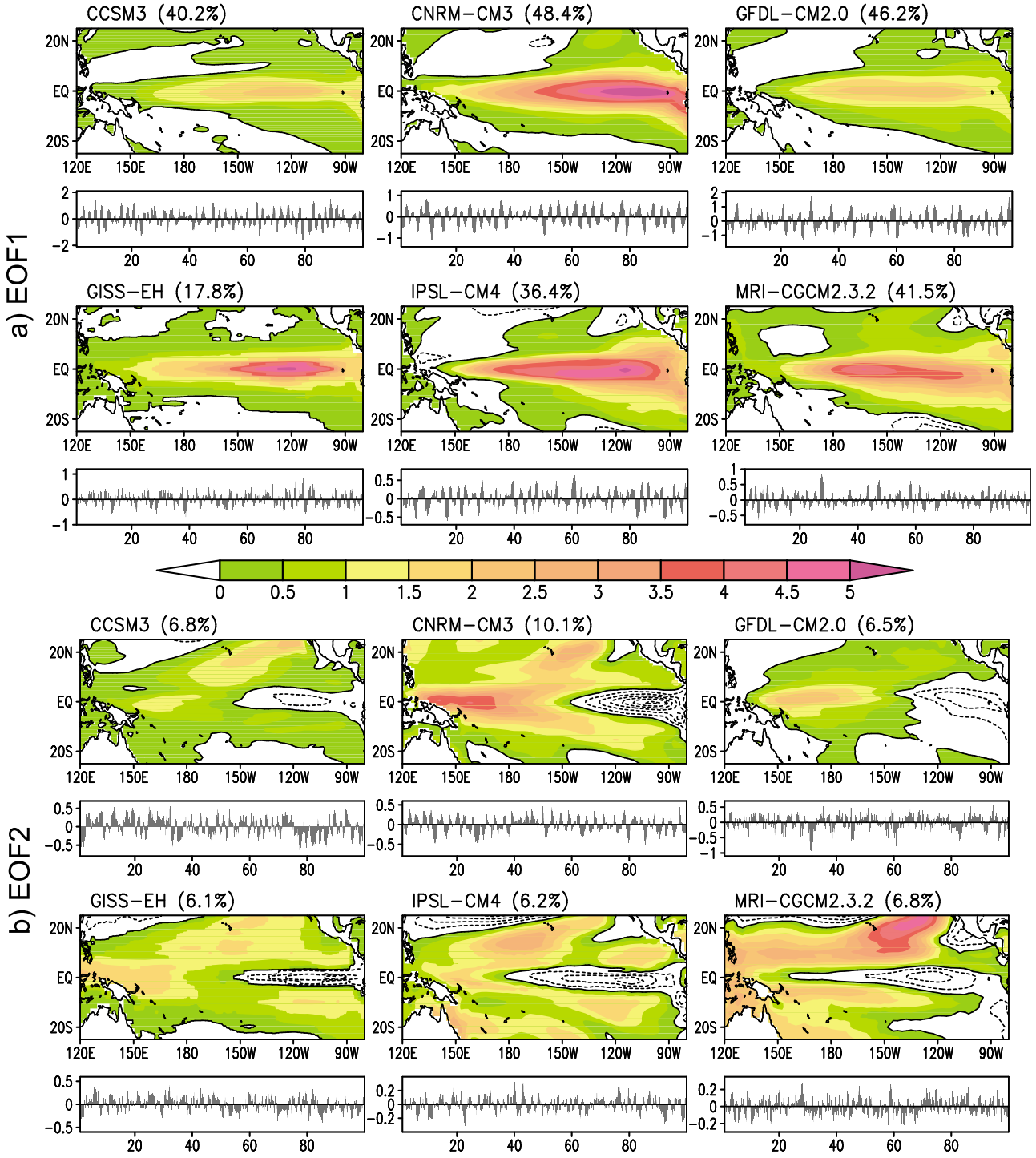

Figure 12. The leading EOF modes in SST in the tropical Pacific (30°S–30°N, 115°E–80°W) and their corresponding PC time series in the picntrl simulations. The dashed line denotes negative values. The contour interval in Figure 12a and Figure 12b is 0.5°C and 1°C, respectively. The models' names and their variances are shown above each EOF mode.

models also suggest the importance of the dynamic feedback in the equatorial Pacific under global warming.

[30] **Acknowledgments.** We thank Fei-Fei Jin for useful discussions during the course of this work. We also appreciate the helpful suggestions and comments from two anonymous reviewers. This work is supported by the National Basic Research Program "973" (grant 2010CB950400) and the National Nature Science Foundation of China (40821092, 41005049).

References

AchutaRao, K., and K. R. Sperber (2002), Simulation of the El Niño Southern Oscillation: Results from the Coupled Model Intercomparison Project, *Clim. Dyn.*, *19*, 191–209, doi:10.1007/s00382-001-0221-9.

AchutaRao, K., and K. R. Sperber (2006), ENSO simulation in coupled ocean-atmosphere models: Are the current models better? *Clim. Dyn.*, *27*, 1–15, doi:10.1007/s00382-006-0119-7.

Ashok, K., S. K. Behera, S. A. Rao, H. Weng, and T. Yamagata (2007), El Niño Modoki and its possible teleconnection, *J. Geophys. Res.*, *112*, C11007, doi:10.1029/2006JC003798.

Brohan, P., J. J. Kennedy, I. Harris, S. F. B. Tett, and P. D. Jones (2006), Uncertainty estimates in regional and global observed temperature changes: A new dataset from 1850, *J. Geophys. Res.*, *111*, D12106, doi:10.1029/2005JD006548.

Cai, W., and P. H. Whetton (2000), Evidence for a time-varying pattern of greenhouse warming in the Pacific Ocean, *Geophys. Res. Lett.*, *27*, 2577–2580, doi:10.1029/1999GL011253.

Cane, M. A. (1998), Climate change: A role for the tropical Pacific, *Science*, *282*, 59–61, doi:10.1126/science.282.5386.59.

Cane, M. A., A. C. Clement, A. Kaplan, Y. Kushnir, D. Pozdnyakov, R. Seager, S. E. Zebiak, and R. Murtugudde (1997), Twentieth-century sea surface temperature trends, *Science*, *275*, 957–960, doi:10.1126/science.275.5302.957.

Carton, J. A., G. Chepurin, X. Cao, and B. Giese (2000), A simple ocean data assimilation analysis of the global upper ocean 1950–95. Part I: Methodology, *J. Phys. Oceanogr.*, *30*, 294–309, doi:10.1175/1520-0485(2000)030<0294:ASODAA>2.0.CO;2.

Chen, D., M. Cane, A. Kaplan, S. Zebiak, and D. Huang (2004), Predictability of El Niño over the past 148 years, *Nature*, *428*, 733–736, doi:10.1038/nature02439.

Clement, A. C., and R. Seager (1999), Climate and the tropical oceans, *J. Clim.*, *12*, 3383–3401, doi:10.1175/1520-0442(1999)012<3383:CATTO>2.0.CO;2.

Clement, A. C., R. Seager, M. A. Cane, and S. E. Zebiak (1996), An ocean dynamical thermostat, *J. Clim.*, *9*, 2190–2196, doi:10.1175/1520-0442(1996)009<2190:AODT>2.0.CO;2.

Collins, M., and the CMIP Modeling Groups (2005), El Niño- or La Niña-like climate change? *Clim. Dyn.*, *24*, 89–104, doi:10.1007/s00382-004-0478-x.

Deser, C., A. S. Phillips, and M. A. Alexander (2010), Twentieth century tropical sea surface temperature trends revisited, *Geophys. Res. Lett.*, *37*, L10701, doi:10.1029/2010GL043321.

Fedorov, A. V., and S. G. Philander (2000), Is El Niño changing?, *Science*, *288*, 1997–2002, doi:10.1126/science.288.5473.1997.

Gillett, N. P., F. W. Zwiers, A. J. Weaver, and P. A. Stott (2003), Detection of human influence on sea-level pressure, *Nature*, *422*, 292–294, doi:10.1038/nature01487.

Gillett, N. P., R. J. Allan, and T. J. Ansell (2005), Detection of external influence on sea-level pressure with a multi-model ensemble, *Geophys. Res. Lett.*, *32*, L19714, doi:10.1029/2005GL023640.

Graham, N. E. (1995), Simulations of recent global temperature trends, *Science*, *267*, 666–671, doi:10.1126/science.267.5198.666.

Hegerl, G. C., F. W. Zwiers, P. Braconnot, N. P. Gillett, Y. Luo, J. A. Marengo Orsini, N. Nicholls, J. E. Penner, and P. A. Stott (2007), Understanding and attributing climate change, in *Climate Change 2007: The Physical Science Basis. Contribution of Working Group I to the Fourth Assessment Report of the Intergovernmental Panel on Climate Change*, edited by S. Solomon, D. Qin, and M. Manning, chap. 9, pp. 663–745, Cambridge Univ. Press, Cambridge, U. K.

Hurrell, J., and K. E. Trenberth (1999), Global sea surface temperature analyses: Multiple problems and their implications for climate analysis, modeling, and reanalysis, *Bull. Am. Meteorol. Soc.*, *80*, 2661–2678, doi:10.1175/1520-0477(1999)080<2661:GSSTAM>2.0.CO;2.

Jin, F.-F., Z.-Z. Hu, M. Latif, L. Bengtsson, and E. Roeckner (2001), Dynamical and cloud-radiation feedbacks in El Niño and greenhouse warming, *Geophys. Res. Lett.*, *28*, 1539–1542, doi:10.1029/2000GL012078.

Kalnay, E., et al. (1996), The NCEP/NCAR 40-year reanalysis project, *Bull. Am. Meteorol. Soc.*, *77*, 437–471, doi:10.1175/1520-0477(1996)077<0437:TNYRP>2.0.CO;2.

Kao, H.-Y., and J.-Y. Yu (2009), Contrasting eastern-Pacific and central-Pacific types of ENSO, *J. Clim.*, *22*, 615–632, doi:10.1175/2008JCLI2309.1.

Kaplan, A., M. A. Cane, Y. Kushnir, A. C. Clement, M. B. Blumenthal, and B. Rajagopalan (1998), Analyses of global sea surface temperature 1856–1991, *J. Geophys. Res.*, *103*, 18,567–18,589, doi:10.1029/97JC01736.

Karnauskas, K. B., R. Seager, A. Kaplan, Y. Kushnir, and M. A. Cane (2009), Observed strengthening of the zonal sea surface temperature gradient across the equatorial Pacific ocean, *J. Clim.*, *22*, 4316–4321, doi:10.1175/2009JCLI2936.1.

Knutson, T. R., and S. Manabe (1995), Time-mean response over the tropical Pacific to increased CO_2 in a coupled ocean-atmosphere model, *J. Clim.*, *8*, 2181–2199, doi:10.1175/1520-0442(1995)008<2181:TMROTT>2.0.CO;2.

Knutson, T. R., and S. Manabe (1998), Model assessments of decadal variability and trend in the tropical Pacific Ocean, *J. Clim.*, *11*, 2273–2296, doi:10.1175/1520-0442(1998)011<2273:MAODVA>2.0.CO;2.

Kug, J.-S., F.-F. Jin, and S.-I. An (2009), Two types of El Niño events: Cold tongue El Niño and warm pool El Niño, *J. Clim.*, *22*, 1499–1515, doi:10.1175/2008JCLI2624.1.

Latif, M., D. Anderson, T. Barnett, M. Cane, R. Kleeman, A. Leetmaa, J. O'Brien, A. Rosati, and E. Schneider (1998), A review of the predictability and prediction of ENSO, *J. Geophys. Res.*, *103*, 14,375–14,393, doi:10.1029/97JC03413.

Lau, K.-M., and H. Weng (1999), Interannual, decadal-interdecadal, and global warming signals in sea surface temperature during 1955–97, *J. Clim.*, *12*, 1257–1267, doi:10.1175/1520-0442(1999)012<1257:IDIAGW>2.0.CO;2.

McPhaden, M. J., S. E. Zebiak, and M. H. Glantz (2006), ENSO as an integrating concept in earth science, *Science*, *314*, 1740–1745, doi:10.1126/science.1132588.

Meehl, G. A., and W. M. Washington (1996), El Niño-like climate change in a model with increased atmospheric CO_2 concentrations, *Nature*, *382*, 56–60, doi:10.1038/382056a0.

Neelin, J. D., M. Latif, and F.-F. Jin (1994), Dynamics of coupled ocean-atmosphere models: The tropical problem, *Annu. Rev. Fluid Mech.*, *26*, 617–659, doi:10.1146/annurev.fl.26.010194.003153.

Noda, A., K. Yamaguchi, S. Yamaki, and S. Yukimoto (1999), Relationship between natural variability and CO_2-induced warming pattern: MRI AOGCM experiment, paper presented at 10th Symposium on Global Change Studies, Am. Meteorol. Soc., Dallas, Tex., 10–15 Jan.

North, G. R., T. L. Bell, B. F. Cahalan, and F. J. Moeng (1982), Sampling errors in the estimation of Empirical Orthogonal Functions, *Mon. Weather Rev.*, *110*, 699–706, doi:10.1175/1520-0493(1982)110<0699:SEITEO>2.0.CO;2.

Philander, S. G. (1990), *El Niño, La Niña, and the Southern Oscillation*, Academic, San Diego, Calif.

Pierrehumbert, R. T. (1995), Thermostats, radiator fins, and the local runaway greenhouse, *J. Atmos. Sci.*, *52*, 1784–1806, doi:10.1175/1520-0469(1995)052<1784:TRFATL>2.0.CO;2.

Rasmusson, E. M., and T. H. Carpenter (1982), Variations in tropical sea surface temperature and surface wind fields associated with Southern Oscillation/El Niño, *Mon. Weather Rev.*, *110*, 354–384, doi:10.1175/1520-0493(1982)110<0354:VITSST>2.0.CO;2.

Rayner, N. A., D. E. Parker, E. B. Horton, C. K. Folland, L. V. Alexander, D. P. Rowell, E. C. Kent, and A. Kaplan (2003), Global analyses of sea surface temperature, sea ice, and night marine air temperature since the late nineteenth century, *J. Geophys. Res.*, *108*(D14), 4407, doi:10.1029/2002JD002670.

Roeckner, E., J. M. Oberhuber, and A. Bacher (1996), ENSO variability and atmospheric response in a global coupled atmosphere-ocean GCM, *Clim. Dyn.*, *12*, 737–754, doi:10.1007/s003820050140.

Seager, R., and R. Murtugudde (1997), Ocean dynamics, thermocline adjustment, and regulation of tropical SST, *J. Clim.*, *10*, 521–534, doi:10.1175/1520-0442(1997)010<0521:ODTAAR>2.0.CO;2.

Smith, T. M., and R. W. Reynolds (2004), Improved extended reconstruction of SST (1854–1997), *J. Clim.*, *17*, 2466–2477, doi:10.1175/1520-0442(2004)017<2466:IEROS>2.0.CO;2.

Sun, D.-Z., and Z. Liu (1996), Dynamic ocean-atmosphere coupling, a thermostat for the tropics, *Science*, *272*, 1148–1150, doi:10.1126/science.272.5265.1148.

Tett, S. F. B. (1995), Simulation of El Niño-Southern Oscillation-like variability in a global AOGCM and its response to CO_2 increase, *J. Clim.*, *8*, 1473–1502, doi:10.1175/1520-0442(1995)008<1473:SOENSO>2.0.CO;2.

Thompson, D. W. J., J. M. Wallace, and G. C. Hegerl (2000), Annular modes in the extratropical circulation. Part II: Trends, *J. Clim.*, *13*, 1018–1036, doi:10.1175/1520-0442(2000)013<1018:AMITEC>2.0.CO;2.

Timmermann, A., J. Oberhuber, A. Bacher, M. Esch, M. Latif, and E. Roeckner (1999), ENSO response to greenhouse warming, *Nature*, *398*, 694–697, doi:10.1038/19505.

Trenberth, K. E., and T. J. Hoar (1996), The 1990–1995 El Niño-Southern Oscillation event: Longest on record, *Geophys. Res. Lett.*, *23*, 57–60, doi:10.1029/95GL03602.

Trenberth, K. E., G. W. Branstator, D. Karoly, A. Kumar, N.-C. Lau, and C. Ropelewski (1998), Progress during TOGA in understanding and modeling global teleconnections associated with tropical sea surface temperature, *J. Geophys. Res.*, *103*, 14,291–14,324.

Wallace, J. M., E. M. Rasmusson, T. P. Mitchell, V. E. Kousky, E. S. Sarachik, and H. von Storch (1998), On the structure and evolution of ENSO-related climate variability in the tropical Pacific: Lessons from TOGA, *J. Geophys. Res.*, *103*, 14,241–14,259, doi:10.1029/97JC02905.

Wang, B. (1995), Interdecadal changes in El Niño onset in the last four decades, *J. Clim.*, *8*, 267–285, doi:10.1175/1520-0442(1995)008<0267:ICIENO>2.0.CO;2.

Wu, Z., B. Wang, J. Li, and F.-F. Jin (2009), An empirical seasonal prediction model of the east Asia summer monsoon using ENSO and NAO, *J. Geophys. Res.*, *114*, D18120, doi:10.1029/2009JD011733.

Yu, J.-Y., and S. T. Kim (2010), Three evolution patterns of Central-Pacific El Niño, *Geophys. Res. Lett.*, *37*, L08706, doi:10.1029/2010GL042810.

Zhang, Y., J. M. Wallace, and D. S. Battisti (1997), ENSO-like interdecadal variability: 1900–93, *J. Clim.*, *10*, 1004–1020, doi:10.1175/1520-0442(1997)010<1004:ELIV>2.0.CO;2.

J. Li and X. Zhao, State Key Laboratory of Numerical Modeling for Atmospheric Sciences and Geophysical Fluid Dynamics, Institute of Atmospheric Physics, Chinese Academy of Sciences, P.O. Box 9804, Beijing 100029, China. (ljp@lasg.iap.ac.cn)

W. Zhang, Key Laboratory of Meteorological Disaster of Ministry of Education and College of Atmospheric Sciences, Nanjing University of Information Science and Technology, Nanjing 210044, China.